# Red-NIR luminescence of $Mo_6$ monolayered assembly directly anchored on Au(001)
# Electronic Supplementary Information

Mikaël Kepenekian,*[a] Yann Molard,[a] Karine Costuas,[a] Pierric Lemoine,[a] Régis Gautier,[a] Soraya Ababou-Girard,[b] Bruno Fabre,[a] Pascal Turban,[b] and Stéphane Cordier*[a]

[a] *Univ Rennes, ENSCR, INSA Rennes, CNRS, ISCR - UMR 6226, F-35000 Rennes, France.*
Email: mikael.kepenekian@univ-rennes1.fr; stephane.cordier@univ-rennes1.fr

[b] *Univ Rennes, CNRS, IPR – UMR 6251, F-35000 Rennes, France.*

## Contents

# 1 Experimental procedures

## 1.1 Cluster synthesis

In the solid state, they are paired with alkali cations (A) to form $A_2[Mo_6X_8^iX_6^a]$ ternary salts.$A_2[Mo_6X_8^iX_6^a]$ salts are soluble and chemically stable in usual solvents like acetone, acetonitrile or water/ethanol mixtures. In the present work, the ternary bromide $Cs_2Mo_6Br_8^iBr_6^a$ was synthesized according to experimental protocol reported in the literature.[1] Then, 1 g of $NH_4(NCS)$ was dissolved in 50 ml of 50/50 water/ethanol under magnetic stirring and 1 g of $Cs_2Mo_6Br_8^iBr_6^a$ was added. After full dissolution, the temperature was increased to 80°C until precipitation of $(NH_4)_2[Mo_6Br_8^i(NCS)_6^a]$. $(NH_4)_2[Mo_6Br_8^i(NCS)_6^a]$ was then dissolved in acetone and $(NH_4)_2[Mo_6Br_8(NCS)_6].4C_3H_6O$ was obtained as single crystals by pentane diffusion. The $[Mo_6X_8^iX_6^a]^{2-}$ cluster anionic unit can be depicted as an octahedral $Mo_6$ cluster face-capped by eight inner bromine ligands forming a $\{Mo_6Br_8^i\}^{4+}$ cluster core. Dried $(NH_4)_2[Mo_6Br_8(NCS)_6]$ powder used for surface deposition and luminescence of bulk samples was obtained by drying of $(NH_4)_2[Mo_6Br_8(NCS)_6].4C_3H_6O$ (100°C, 12 h). Structural data collection and analysis are summarized below.

## 1.2 X-ray Crystallography

Single crystal X-ray diffraction data were collected at 150 K on a D8 Venture Bruker AXS diffractometer using a Mo-K$\alpha$ X-ray wavelength of $\lambda$=0.71073 Å and processed with the APEX 3 program suite.[2] Frame integration and data reduction were carried out with the program SAINT.[3] The program SADABS[4] was employed for multiscan-type absorption corrections. The structures were solved by direct methods using the SIR97 program[5] and refined with full-matrix least-squares methods based of $F^2$ (SHELXL)[6] through the aid of the WinGX platform.[7] All non-hydrogen atoms were refined with anisotropic atomic displacement parameters. Hydrogen atoms arising from acetone molecules were included in the structural model considering their calculated positions and their equivalent isotropic displacement parameters were constrained to be equal to 1.5 times that of the carbon atom. Hydrogen atoms arising from ammonium cation were not included in the structural model. The non-negligible largest differences peak and hole electron density (*i.e.* 3.69 $e^-.Å^{-3}$ and $-4.07$ $e^-.Å^{-3}$) are located at the proximity of the heavy $\{Mo_6Br_8\}$ cluster core and are attributed to weak structural disorder. Publishing data were computed using CRYSCALC program [T. Roisnel, local program, www.cdifx.univ-rennes1.fr/cryscalc]. The crystallographic data were deposited with the Cambridge Crystallographic Data Centre (CCDC 1901701).

## 1.3 Preparation of Au(001)

Au(001) films were prepared by molecular beam epitaxy. First a 60 nm thick Fe(001) film was grown on a MgO(001) commercial single crystal at room temperature. A post growth annealing at 800 K was used to smooth the surface.[8] Finally a 10 nm Au(001) layer was epitaxially grown on the previous Fe(001) surface at room temperature. The resulting Au(001) surface observed by scanning tunneling microscopy (STM, Figure S3) presents a root-mean square roughness of 0.46 nm and extended atomic terraces running along the [110] and [1-10] direction of the Au crystal, with typical lateral size larger than 100 nm.

## 1.4 Cluster deposition

The procedure used for the deposition of $[Mo_6Br_8^i(NCS)_6^a]^{2-}$ onto gold was similar to that use by Prokopuk and Shriver for the deposition of $[Nb_6X_{12}^i(NCS)_6^a]^{4-}$ onto gold (see ESI†).[9] 3.99 mg of $(NH_4)_2[Mo_6Br_8^i(NCS)_6^a]$ were dissolved in 25 $cm^3$ of $CH_2Cl_2$ along with few drops of absolute ethanol to obtain a 0.1 mM solution. The solution was degassed, put under argon and then the gold surface was immersed. Note that a teflon platform at the bottom of the schlenk flask enabled to prevent contacts between the magnetic stirrer and the surface. After 12 h, the surface was recovered and dried on air.

## 1.5 Atomic Force Microscopy

AFM images were acquired on a Cypher Asylum microscope in tapping mode with FM tips (resonance frequency around 239 kHz). The images were treated and analyzed with the open-source Gwyddion (version 2.52) software.

## 1.6 Electrochemical Measurements

Cyclic voltammograms were recorded in dry $CH_2Cl_2$ using an Autolab electrochemical analyzer (PGSTAT 30 potentiostat/galvanostat from Eco Chemie B.V.) equipped with the GPES software in a three-electrode glass cell. The working electrode was either a 1 mm-diameter Pt disk for the dissolved cluster or a $[Mo_6Br_8(NCS)_6]$-modified gold surface (surface area of 0.20 $cm^2$), the counter electrode a glassy carbon rod, and the reference electrode a Ag wire dipped into an acetonitrile solution containing $10^{-2}$ M $AgNO_3$. The ferrocene/ferrocenium couple ($E^{\circ\prime}$=0.18 V *vs.* $10^{-2}$ M $Ag^+$/Ag, $\Delta E_p$=0.08 V; $I_{pa}/I_{pc}$=1) was used as an internal calibrant for the potential measurements.[10] Tetra-*n*-butylammonium hexafluorophosphate *n*-$Bu_4NPF_6$ was purchased from Sigma-Aldrich (puriss, electrochemical grade) and was used at 0.2 M as supporting electrolyte in $CH_2Cl_2$ (anhydrous, analytical grade from SDS). The ($CH_2Cl_2$ + 0.2 M *n*-$Bu_4NPF_6$) electrolytic medium was dried over activated, neutral alumina (Merck) for 30 min., under stirring, and under argon. Alumina was previously activated at 450°C under vacuum for several hours. All electrochemical measurements were carried out inside a home-made Faraday cage at room temperature (20$\pm$2°C) and under a constant flow of argon.

## 1.7 Scanning Tunneling Microscopy

STM data were acquired using an OMICRON VT STM microscope in an ultrahigh vacuum chamber at a base pressure lower than $10^{-10}$ mbar. Tungsten tips were electrochemically etched in a NaOH solution (5 M) and cleaned in situ by thermal heating to remove the oxide layer before experiments. Samples were grounded by an ohmic contact on the Au layer surface ($V_{sample}$=0). The applied tunnel voltage is defined as $V_T$=$V_{sample}$-$V_{tip}$=$-V_{tip}$, and the tunnel current is denoted as $I_T$. Freshly grafted samples were promptly transferred from the ambient to ultrahigh vacuum after molecular grafting and degassed for 1 hour at 400 K to remove traces of water contamination and improve the tip-sample tunnel contact. All experiments took place at room temperature. STM images were acquired at room temperature and in the constant current mode and were only postprocessed with a background plane correction. STS measurements were made by recording single $I_T(V_T)$ curve on individual $[Mo_6Br_8(NCS)_6]^{2-}$ grafted cluster while keeping the tip/sample distance constant.

## 1.8 X-ray Photoemission Spectroscopy

XPS measurements were performed with an Mg K$\alpha$ ($h\nu$) anode, at 1254 eV X-ray energy, using a VSW HA100 photoelectron spectrometer with a hemispherical photoelectron analyzer, working at an energy pass of 20 eV for survey and resolved spectra. The experimental resolution was 1.0 eV. The binding energy scale of the XPS is such that the $Au4f_{7/2}$ peak is set at 84.0$\pm$0.1 eV, all the given binding energies being then referred to the Fermi level at the surface. Experimental data were fitted after Shirley background subtraction, with a mixed of Gaussian-Lorentzian shape.

## 1.9 Periodic Density Functional Theory

Periodic first-principles calculations are based on DFT as implemented in the SIESTA package.[11,12] Calculations have been carried out with the GGA functional in the revPBE form,[13] Troullier-Martins pseudopotentials,[14] and a basis set of finite-range numerical pseudoatomic orbitals for the valence wave functions.[15] Structures relaxation and electronic structure calculations have been done using a double-$\zeta$ polarized basis sets.[15] The electronic structure was converged using a 3$\times$3$\times$1 *k*-point sampling of the Brillouin zone. In all cases, an

energy cutoff of 400 Ry for real-space mesh size has been used. $[Mo_6Br_8(NCS)_6]^{2-}$ units are deposited on a 5-layer slab of the Au(001) surface. The bottom 3 layers are kept frozen along the relaxation process, while the top 2 layers are allowed to move until forces are smaller than 0.01 eV/Å.

## 1.10 Photoluminescence Measurements

Spectra were recorded with a home-made setup consisting of an optical Nikon 80i microscope equipped with a Linkam LTS420 hot stage, a Nikon Hg Intensilight irradiation source presenting a bandwidth ranging from 380 to 420 nm and an Ocean Optics QE6500 photodetector connected by optical fiber. Measurements are performed in the solid state from T=80 K to room temperature with an increment of 20 K under $N_2$ atmosphere. Acquisition times for the surface alone and the modified surface were 40 s while it took only 10 ms to get the cluster powder signal emission profile. Emission intensities have been normalized to compare the maxima position. The depletion observed at 945 nm in all cases is an artifact due to the absorption of the optical fiber.

## 1.11 Molecular DFT and TD-DFT

Molecular DFT calculations were carried out using the Amsterdam Density Functional (ADF 2016) package developed by Baerends and coworkers.[16,17] The revPBE exchange and correlation non-local gradient corrections were added to the local density approximation functional.[13] Relativistic effects were treated at the first-order of perturbation theory using a ZORA Hamiltonian.[18,19] The all-electron ADF QZ4P Slater-type atomic basis set has been used, *i.e.* a quadruple-ζ STO basis set completed with four polarization functions. This procedure was successfully employed to study ground and excited state geometries and optical properties of the parent $[Mo_6Br_{14}]^{2-}$ metal cluster in good agreement with experimental results.[20] The quality of atomic basis set and the use of relativistic effect correction makes the level of theory of this molecular computational study higher than the one used in the calculations of surface for which this higher level of theory is not affordable. Such a level of theory is compulsory for the molecular computational investigations to obtain sufficiently precise photophysical calculated values that allow comparisons with experimental results.

# 2 Results

## 2.1 X-ray crystallographic study

Crystal data:crystal size = 0.21×0.07×0.04 $mm^3$, crystal color: yellow, space group $Pccn$, T = 150(2) K, a = 21.7258(20) Å, b = 13.1123(11) Å, c = 17.0196(15) Å, V = 4848.5(12) $Å^3$, Z = 4, empirical formula: $C_{18}H_{32}Br_8Mo_6N_8O_4S_6$, $M_f$=1831.79 $g.mol^{-1}$, $\rho_{calc}$=2.509 $g.cm^{-3}$, F(000) = 3424, $\theta$ range for data collection: 3.004 - 27.538° (h_min, h_max: -28, 28 ; k_min, k_max: -17, 15 ; l_min, l_max: -22, 22), 26105 reflections collected, 5580 unique reflections, $R_{int}$=0.1138, completeness to theta max = 0.997, 228 refined parameters, 12 restraint parameters, Goodness-of-fit = 1.117, final $R_1$ [I > 2$\sigma$] = 0.1073, final $wR_2$ [I > 2$\sigma$] = 0.2389, largest difference peak and hole: +3.686 and -4.074 e.$Å^{-3}$.

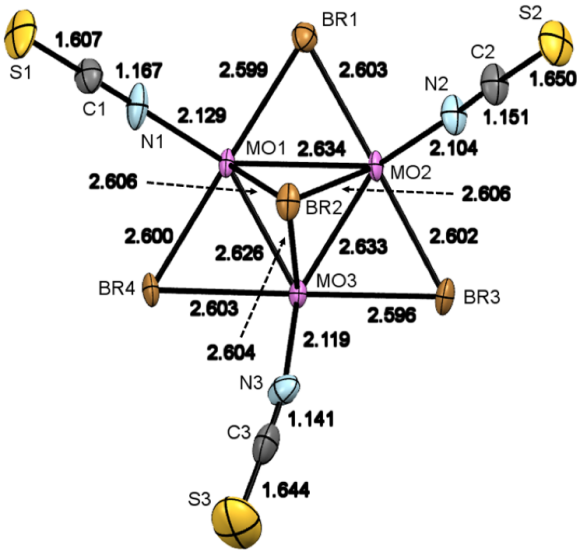


**Figure S1.** Representation of the asymmetric cluster unit $[Mo_6Br_8(NCS)_6]^{2-}$ with corresponding interatomic distances at 150 K for $(NH_4)_2[Mo_6Br_8(NCS)_6].4C_3H_6O$.

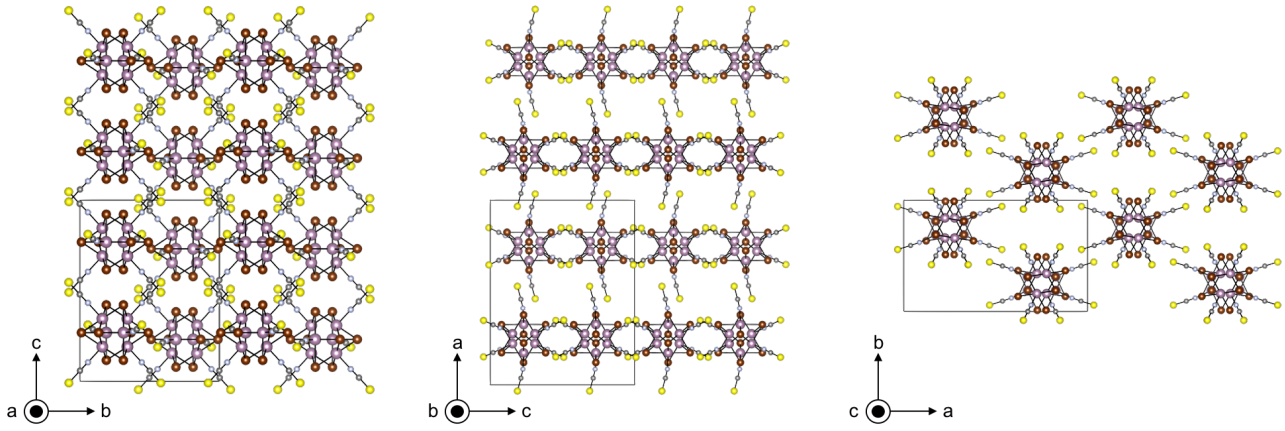


**Figure S2.** $(NH_4)_2[Mo_6Br_8(NCS)_6].4C_3H_6O$ crystal packing. For clarity, $NH_4$ and $C_3H_6O$ are not depicted. Mo, Br, S, N and C atoms are depicted in violet, brown, yellow, blue and gray, respectively.

**Table S1.** Atomic coordinates, site occupancy and equivalent isotropic displacement parameters refined at 150 K for $(NH_4)_2[Mo_6Br_8(NCS)_6].4(C_3H_6O)$.

| Atom | Site | x | y | z | Occ. | U(eq) |
|---|---|---|---|---|---|---|
| cluster unit $[Mo_6Br_8(NCS)_6]^{2-}$ | | | | | | |
| Mo1 | 8e | 0.2233(2) | 0.6598(2) | 0.1542(2) | 1.00 | 0.0163(4) |
| Mo2 | 8e | 0.2233(2) | 0.6597(2) | 0.3089(2) | 1.00 | 0.0183(4) |
| Mo3 | 8e | 0.3267(1) | 0.6879(2) | 0.2312(2) | 1.00 | 0.0174(4) |
| Br1 | 8e | 0.1212(2) | 0.6340(2) | 0.2313(2) | 1.00 | 0.0274(5) |
| Br2 | 8e | 0.2736(2) | 0.5098(2) | 0.2315(2) | 1.00 | 0.0257(5) |
| Br3 | 8e | 0.3262(2) | 0.6889(2) | 0.3838(2) | 1.00 | 0.0272(6) |
| Br4 | 8e | 0.3258(2) | 0.6886(2) | 0.0783(2) | 1.00 | 0.0224(5) |
| N1 | 8e | 0.1912(12) | 0.5563(16) | 0.0670(12) | 1.00 | 0.036(6) |
| C1 | 8e | 0.1746(13) | 0.4976(19) | 0.0200(15) | 1.00 | 0.032(6) |
| S1 | 8e | 0.1513(5) | 0.4191(7) | -0.0461(5) | 1.00 | 0.057(3) |
| N2 | 8e | 0.1929(11) | 0.5566(15) | 0.3954(12) | 1.00 | 0.031(5) |
| C2 | 8e | 0.1741(14) | 0.4997(19) | 0.4410(15) | 1.00 | 0.034(6) |
| S2 | 8e | 0.1494(4) | 0.4199(7) | 0.5090(5) | 1.00 | 0.051(2) |
| N3 | 8e | 0.4151(10) | 0.6201(16) | 0.2263(14) | 1.00 | 0.033(5) |
| C3 | 8e | 0.4636(16) | 0.592(2) | 0.2125(15) | 1.00 | 0.043(7) |
| S3 | 8e | 0.5336(5) | 0.5562(9) | 0.1884(7) | 1.00 | 0.080(3) |
| $(NH_4)^+$ counter cations | | | | | | |
| N4 | 4a | 0 | 0 | 0 | 1.00 | 0.058(11) |
| N5 | 4c | $\frac{1}{4}$ | $\frac{1}{4}$ | 0.059(3) | 1.00 | 0.073(13) |
| Acetone molecules | | | | | | |
| C4 | 8e | 0.512(2) | 0.285(4) | 0.526(3) | 1.00 | 0.089(16) |
| C5 | 8e | 0.514(2) | 0.309(4) | 0.440(3) | 1.00 | 0.104(18) |
| H5A | 8e | 0.503 | 0.379 | 0.432 | 1.00 | 0.156 |
| H5B | 8e | 0.555 | 0.299 | 0.420 | 1.00 | 0.156 |
| H5C | 8e | 0.486 | 0.266 | 0.412 | 1.00 | 0.156 |
| C6 | 8e | 0.506(3) | 0.376(5) | 0.579(4) | 1.00 | 0.13(2) |
| H6A | 8e | 0.495 | 0.435 | 0.549 | 1.00 | 0.197 |
| H6B | 8e | 0.475 | 0.363 | 0.617 | 1.00 | 0.197 |
| H6C | 8e | 0.545 | 0.388 | 0.606 | 1.00 | 0.197 |
| O1 | 8e | 0.525(2) | 0.202(3) | 0.547(3) | 1.00 | 0.127(14) |
| C7 | 8e | 0.132(3) | 0.234(3) | 0.231(3) | 1.00 | 0.077(13) |
| C8 | 8e | 0.077(2) | 0.161(4) | 0.235(3) | 1.00 | 0.11(2) |
| H8A | 8e | 0.060 | 0.153 | 0.184 | 1.00 | 0.171 |
| H8B | 8e | 0.091 | 0.096 | 0.255 | 1.00 | 0.171 |
| H8C | 8e | 0.047 | 0.189 | 0.270 | 1.00 | 0.171 |
| C9 | 8e | 0.166(3) | 0.262(5) | 0.289(4) | 1.00 | 0.16(3) |
| H9A | 8e | 0.151 | 0.232 | 0.337 | 1.00 | 0.236 |
| H9B | 8e | 0.208 | 0.241 | 0.280 | 1.00 | 0.236 |
| H9C | 8e | 0.165 | 0.335 | 0.294 | 1.00 | 0.236 |
| O2 | 8e | 0.154(3) | 0.277(7) | 0.168(4) | 1.00 | 0.26(4) |

**Table S2.** Bond lengths (Å), bond angles (°) and torsion angles (°) at 150 K in the cluster unit $[Mo_6Br_8(NCS)_6]^{2-}$.

| | | | | | | | |
|---|---|---|---|---|---|---|---|
| Mo1-Mo1[a] | 2.633 | Mo1-Br1 | 2.599 | Mo1-N1 | 2.129 | Mo1-N1-C1 | 178.22 |
| Mo1-Mo2 | 2.634 | Mo1-Br2 | 2.606 | Mo2-N2 | 2.104 | Mo2-N2-C2 | 177.18 |
| Mo1-Mo3 | 2.626 | Mo1-Br4 | 2.600 | Mo3-N3 | 2.119 | Mo3-N3-C3 | 168.96 |
| Mo1-Mo3[a] | 2.624 | Mo1-Br4[a] | 2.599 | ($d_{(Mo-N)}$) | 2.117 | N1-C1-S1 | 178.52 |
| Mo2-Mo2[a] | 2.638 | Mo2-Br1 | 2.603 | N1-C1 | 1.167 | N2-C2-S2 | 177.53 |
| Mo2-Mo3 | 2.633 | Mo2-Br2 | 2.606 | N2-C2 | 1.151 | N3-C3-S3 | 176.53 |
| Mo2-Mo3[a] | 2.631 | Mo2-Br3 | 2.602 | N3-C3 | 1.143 | Mo1-N1-C1-S1 | -155.49 |
| ($d_{(Mo-Mo)}$) | 2.631 | Mo2-Br3a | 2.592 | ($d_{(N-C)}$) | 1.154 | Mo2-N2-C2-S2 | -164.08 |
| | | Mo3-Br1[a] | 2.594 | C1-S1 | 1.607 | Mo3-N3-C3-S3 | +10.58 |
| | | Mo3-Br2 | 2.604 | C2-S2 | 1.650 | | |
| | | Mo3-Br3 | 2.596 | C3-S3 | 1.642 | | |
| | | Mo3-Br4 | 2.603 | ($d_{(C-S)}$) | 1.633 | | |
| | | ($d_{(Mo-Br)}$) | 2.600 | | | | |

Symmetry codes: (a) $\frac{1}{2} - x$, $1.5 - y$, $z$

**Table S3.** Short contact distances (Å) and hydrogen bonds geometries at 150 K in $(NH_4)_2[Mo_6Br_8(NCS)_6].4(C_3H_6O)$.

| | | | | |
|---|---|---|---|---|
| Br1···S3[a] | 3.424 | S2···N5[c] | 3.236 | |
| Br3···Br4[b] | 3.680 | O1···N4[e] | 2.819 | |
| Br3···C1[c] | 3.417 | O2···N5 | 2.805 | |
| Br4···C2[d] | 3.405 | | | |
| D-H···A | D···A (Å) | D-H (Å) | H···A (Å) | D-H···A (°) |
| C5-H5B···Br4[f] | 3.835 | 0.96 | 2.97 | 151 |
| C6-H6C···Br3[g] | 3.793 | 0.96 | 2.99 | 142 |
| C8-H8B···C3[h] | 3.457 | 0.96 | 2.83 | 124 |
| C9-H9A···S1[i] | 3.688 | 0.96 | 2.81 | 153 |

Symmetry codes: (a) $-\frac{1}{2} + x$, $1 - y$, $\frac{1}{2} - z$ ; (b) $x$, $1.5 - y$, $\frac{1}{2} + z$
(c) $\frac{1}{2} - x$, $y$, $\frac{1}{2} + z$ ; (d) $\frac{1}{2} - x$, $y$, $-\frac{1}{2} + z$ ; (e) $\frac{1}{2} + x$, $-y$, $\frac{1}{2} - z$ ;
(f) $1 - x$, $-\frac{1}{2} + y$, $\frac{1}{2} - z$ ; (g) $1 - x$, $1 - y$, $1 - z$ ;
(h) $\frac{1}{2} - x$, $\frac{1}{2} - y$, $z$ ; (i) $x$, $\frac{1}{2} - y$, $\frac{1}{2} + z$

## 2.2 Scanning Tunneling Microscopy and Atomic Force Microscopy

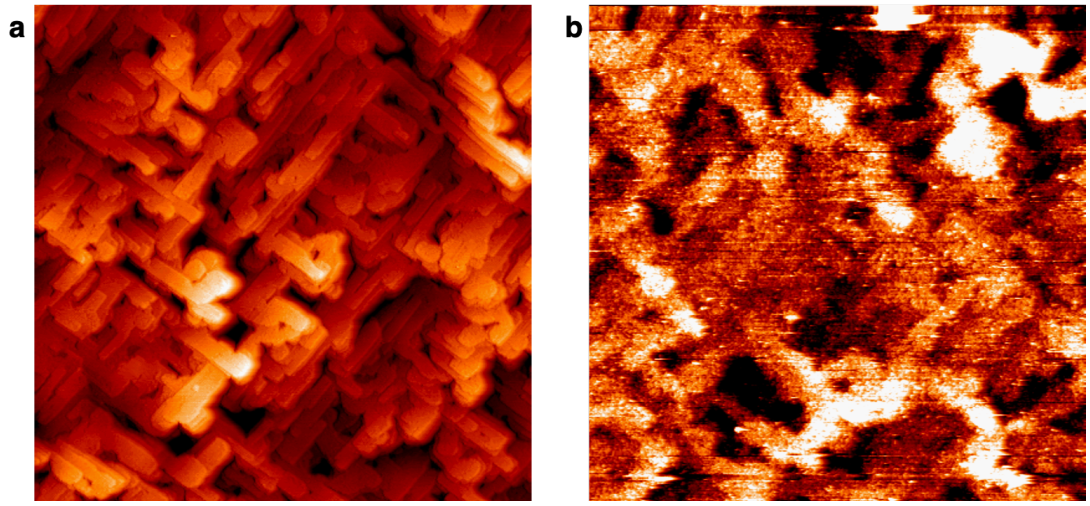


**Figure S3.** 400×400 nm$^2$ Constant current STM images of **a** the bare Au(001) surface (color scale : 0-4.8 nm), and **b** $[Mo_6Br_8(NCS)_6]^{2-}$ grafted Au(001) surface (color scale : 0-5.1nm).

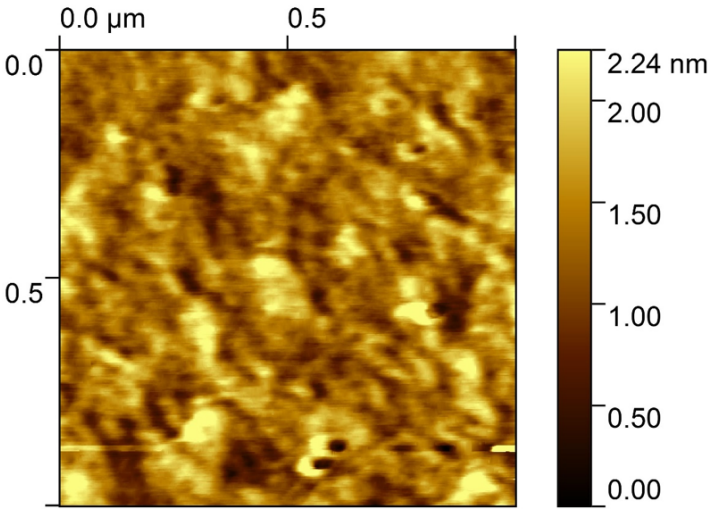


**Figure S4.** 1×1 $\mu$m$^2$ AFM image of the $[Mo_6Br_8^i(NCS)_6^a]$-Au(001) surface.

## 2.3 Electrochemistry

The experimental separation $\Delta E_{p/2}$ between the cathodic peak potential ($E_{pc/2}$) and the half-peak potential ($E_{pc/2}$) is equal to 84 mV. Theoretically, for a totally irreversible wave, $E_{p/2}$ is equal to $(1.857RT)/(\alpha n_a F)$ where $R$ is the gas constant, $T$ the temperature, $\alpha$ the charge transfer coefficient, $n_a$ the number of electrons involved in the rate-determining step and $F$ the Faraday constant. At 293 K and assuming $\alpha$=0.5, we find $n_a$=1.1 which would indicate a one-electron redox process.

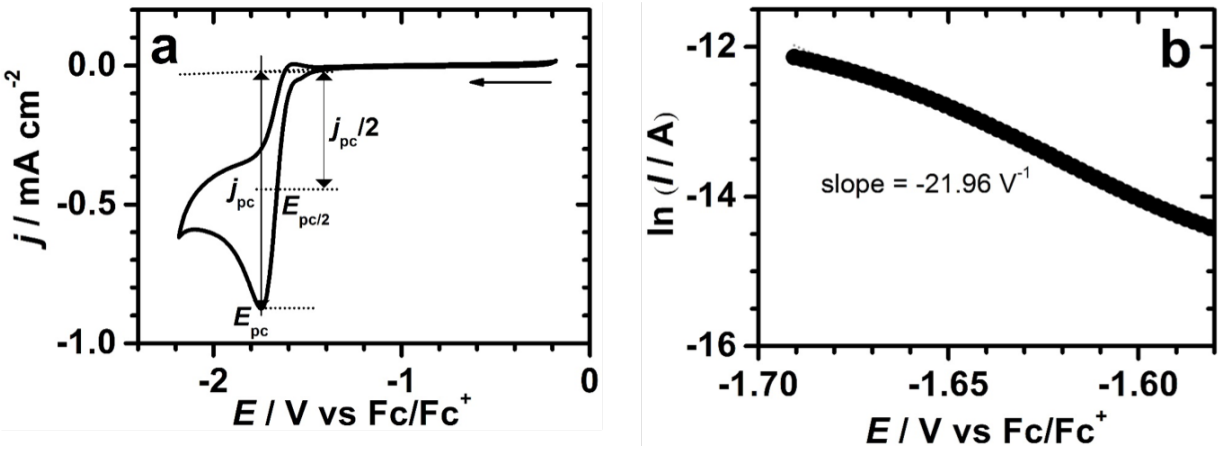


**Figure S5.** **a** Cyclic voltammograms at 0.1 V.s$^{-1}$ of ($n$-$Bu_4N$)$_2$[$Mo_6Br_8(NCS)_6$] at 2 mM on Pt disk electrode. Electrolytic solution: $CH_2Cl_2$ + 0.2 M $Bu_4NPF_6$. **b** Corresponding Tafel plot (ln(I) *vs.* E).

This is confirmed by the Tafel analysis of the cathodic part (Figure **S5**b). A Tafel plot (ln(I) *vs.* E) gives a linear slope of -21.96 V$^{-1}$ which is close to the theoretical value of 19.8 V$^{-1}$ expected for a monoelectronic process ($-\alpha nF/RT$) assuming that $\alpha$=0.5 and T=293 K.[21]

## 2.4 Scanning Tunneling Spectroscopy

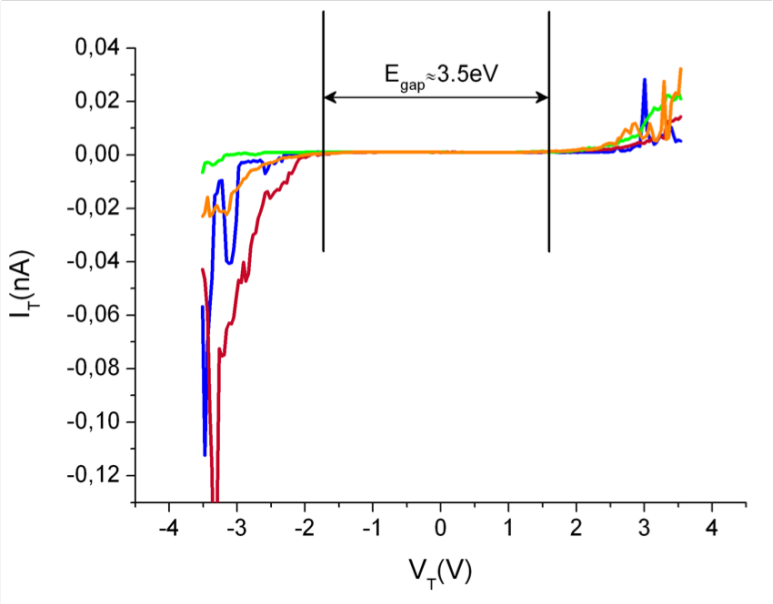


**Figure S6.** Scanning tunneling spectra of the $[Mo_6Br_8^i(NCS)_6^a]^{2-}$ monolayer supported on Au(001).

## 2.5 Periodic Density Functional Theory

**Table S4.** Total energy (eV) of the relaxed structures obtained for $[Mo_6Br_8(NCS)_6]^{2-}$ supported on the Au(001) surface for various numbers of anchors and type of the anchoring sites (top, bridge, hollow).

| | Site | Total energy (eV) |
|---|---|---|
| 1 anchor | hollow | 6.34 |
| 2 anchors | top | 2.17 |
| 3 anchors | hollow | 1.48 |
| 4 anchors | bridge | 0 |

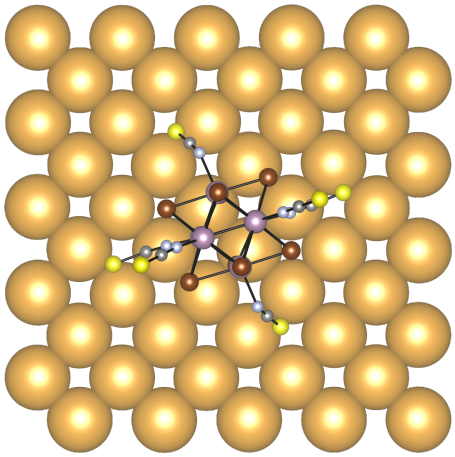

**Figure S7.** Top view of the 4-anchor relaxed configuration on Au(001). For clarity, only the first gold layer is depicted. Au, Mo, Br, S, N and C atoms are depicted in gold, violet, brown, yellow, blue and gray, respectively.

## 2.6 Photoluminescence

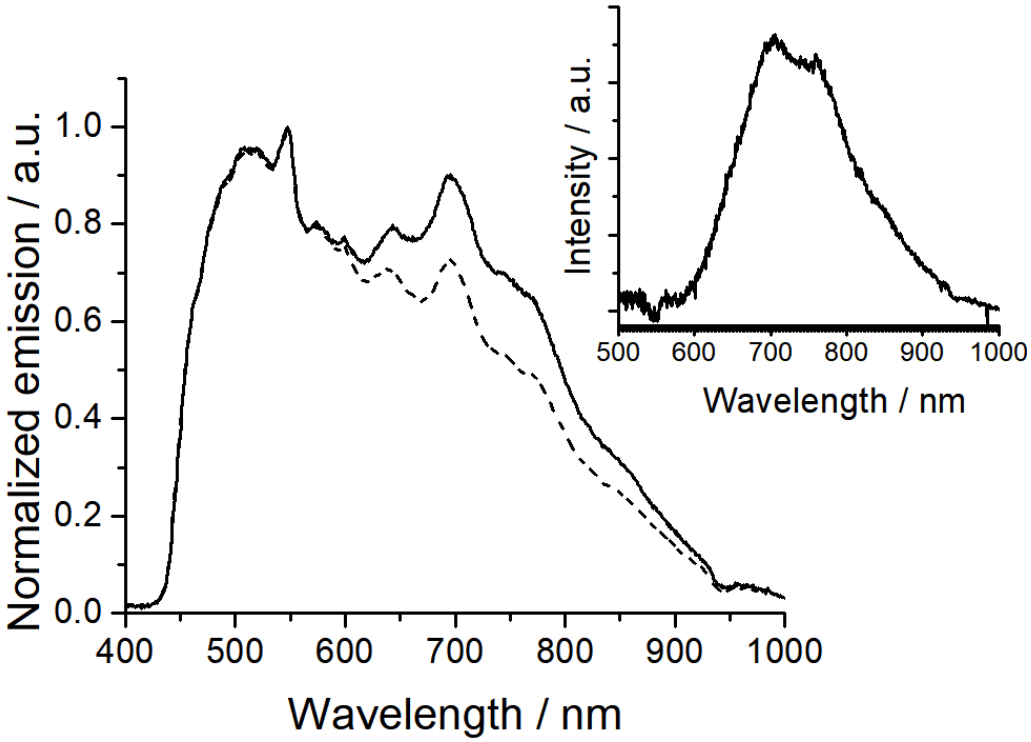


**Figure S8.** Luminescence spectra taken at T=20°C for the bare Au(001) surface (dashed line) and the $Mo_6$-grafted gold surface (plain line). In inset the difference between both signals is plotted.

## 2.7 Molecular DFT and TD-DFT calculations

Since important decrease of symmetry of the excited state arrangements were found for $[Mo_6Br_{14}]^{2-}$ compare to the ground state ($O_h$ symmetry), we choose not to impose symmetry in the present study to tackle the absorption and emission properties of the $[Mo_6Br_8(NCS)_6]^{2-}$ molecular unit. Geometry optimizations of the free ground state ($S_0$) and triplet excited states of $[Mo_6Br_8(NCS)_6]^{2-}$ were performed. For the triplet excited states ($T_n$) investigations, both the default geometry minimization procedure provided in ADF (different initial molecular arrangements) and using analytical time-dependent DFT gradients (TD geometry optimizations of the 12 first excitations). Vibrational frequency calculations were performed to check the local minimum character of all arrangements.

The metal-metal distances of the molecular optimized geometry of $S_0$ are 0.016 Å shorter (Mo-Mo distances of 2.660 Å) than the ones of the optimized $S_0$ arrangement obtained using the periodic computational approach. The metal ligand distances are also affected by this use higher level of theory for the molecular investigations (larger atomic basis set and the partial consideration of the relativistic effects through ZORA) with lengthenings of 0.053 Å of the Mo-Br bonds and of 0.019 Å of the Mo-N bonds, leading to distances of 2.655 Å and 2.103 Å, respectively. The metal-metal distances obtained by this molecular DFT calculation are closer to the one observed in the crystal structure of $(NH_4)_2Mo_6Br_8(NCS)_6.4C_3H_6O$ in which the $Mo_6Br_8(NCS)_6$ motive show a $D_{3d}$ symmetry with a Mo-Mo average distance of 2.631 Å. They are also in agreement with previously reported calculations, slight differences being assigned to the use of smaller basis sets (TZ2P) in that study.[22]

**Table S5.** Mo-Mo bond lengths of the optimized geometries $S_0$, $T_1$, $T_2$, $T_3$, $^{const}S_0$, $^{const}T_1$ and $^{const}T_2$. Atom labels are defined on Figure **S9**. Distances varying of more than 1.4% from its related singlet are in bold style.

| Atoms | $S_0$ | $T_1$ | $T_2$ | $T_3$ | $^{const}S_0$ | $^{const}T_1$ | $^{const}T_2$ |
|---|---|---|---|---|---|---|---|
| $Mo_1$-$Mo_2$ | 2.660 | 2.664 | 2.665 | **3.070** | 2.679 | **2.779** | **2.834** |
| $Mo_4$-$Mo_3$ | 2.660 | 2.664 | 2.668 | 2.685 | 2.647 | 2.645 | 2.644 |
| $Mo_1$-$Mo_4$ | 2.660 | 2.640 | 2.634 | 2.678 | 2.653 | 2.653 | 2.696 |
| $Mo_2$-$Mo_3$ | 2.660 | 2.637 | 2.647 | 2.676 | 2.654 | **2.712** | 2.650 |
| $Mo_5$-$Mo_1$ | 2.660 | **2.741** | **2.767** | **2.717** | 2.647 | 2.612 | **2.715** |
| $Mo_5$-$Mo_2$ | 2.660 | **2.747** | **2.721** | **2.721** | 2.613 | **2.740** | 2.630 |
| $Mo_5$-$Mo_3$ | 2.660 | **2.752** | **2.715** | 2.642 | 2.673 | 2.652 | 2.673 |
| $Mo_5$-$Mo_4$ | 2.660 | **2.738** | **2.765** | 2.646 | 2.668 | 2.668 | 2.658 |
| $Mo_6$-$Mo_1$ | 2.660 | 2.657 | 2.656 | **2.720** | 2.614 | 2.676 | **2.571** |
| $Mo_6$-$Mo_2$ | 2.660 | 2.660 | 2.660 | **2.718** | 2.652 | **2.565** | **2.687** |
| $Mo_6$-$Mo_3$ | 2.660 | 2.658 | 2.661 | 2.643 | 2.667 | **2.707** | 2.691 |
| $Mo_6$-$Mo_4$ | 2.660 | 2.658 | 2.657 | 2.645 | 2.673 | 2.682 | **2.703** |
| *average* | *2.660* | *2.685* | *2.685* | *2.713* | *2.653* | *2.674* | *2.679* |

For $T_1$, the elongation occurred along the C4 axis and induced a lengthening of 0.085 Å of the distances between the Mo atoms of the basal plane ($Mo_{basal(1,2,3,4)}$) an the apex Mo atom ($Mo_{apex(5)}$) compared with the distances of ground state geometry (final average $Mo_{apex}$-$Mo_{basal}$ = 2.745 Å, left arrangement of Figure **S9**). For $T_2$, the elongation lead to the loss of the $C_4$ symmetry axis and resulted in two sets of two $Mo_{apex}$-$Mo_{basal}$ average distances, *i.e.* 2.766 and 2.718 Å (see central arrangement of Figure **S9**). Finally, a higher-lying triplet $[Mo_6Br_8(NCS)_6]^{2-}$ arrangement, namely $T_3$, can be described as the result of the elongation of one $Mo_{basal}$-$Mo_{basal}$ bond from 2.660 Å (in $S_0$) to 3.070 Å (see right arrangement of Figure **S9**). It leads consequently to a partial remoteness of those two $Mo_{basal}$ atoms with the two molybdenum apexes (2.719 Å). The bridging bromine atoms and NCS ligands move consequently to these changes. This excited state geometry reorganization was also found for $[Mo_6Br_{14}]^{2-}$.

In order to mimic the effect of surface grafting, partial geometry optimizations of the $[Mo_6Br_8(NCS)_6]^{2-}$ geometry extracted from the surface computational studies were performed. The carbon and sulfur atomic

positions of the NCS ligands in interaction with the gold surface were kept fixed. Thus 4 NCS groups were frozen giving rise to $^{const}S_0$ for the singlet state and $^{const}T_1$ for the excited triplet state. A second geometry optimization of a 4-anchored triplet states was performed by fixing only the four sulfur positions previously mentioned in order to introduce some flexibility that most probably exists during the relaxation process of the triplet excited states. The resulting excited triplet state is labelled $^{const}T_2$. Il all cases, tight convergence criteria were used for these constrained geometry optimizations (energy change $<$0.0001 u.a., atomic position displacement $<$0.001 Å).

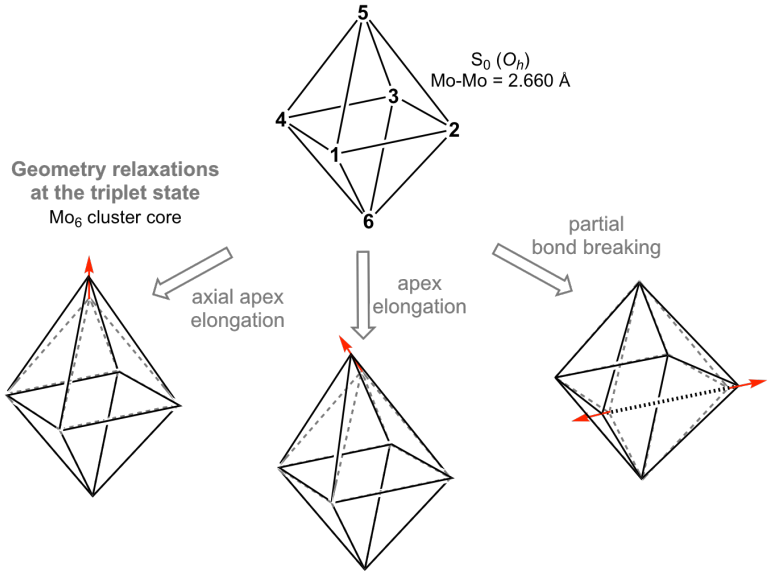


**Figure S9.** TD-DFT geometry relaxation at the triplet state for the free-standing $[Mo_6Br_8(NCS)_6]^{2-}$ molecule.

**Table S6.** TD-DFT calculated emission wavelengths $\lambda_{em}$ (nm and emission energies (eV) for $T_1$, $T_2$, $T_3$ obtained without any geometrical constraint imposed on $[Mo_6Br_8(NCS)_6]^{2-}$, and $^{const}T_1$ and $^{const}T_2$ obtained by mimicking the geometry of the grafted species.

| | $\lambda_{em}$ (nm) | $\lambda_{em}$ (eV) |
|---|---|---|
| $T_1$ | 707 | 1.756 |
| $T_2$ | 720 | 1.724 |
| $T_3$ | 873 | 1.420 |
| $^{const}T_1$ | 794 | 1.563 |
| $^{const}T_2$ | 838 | 1.482 |

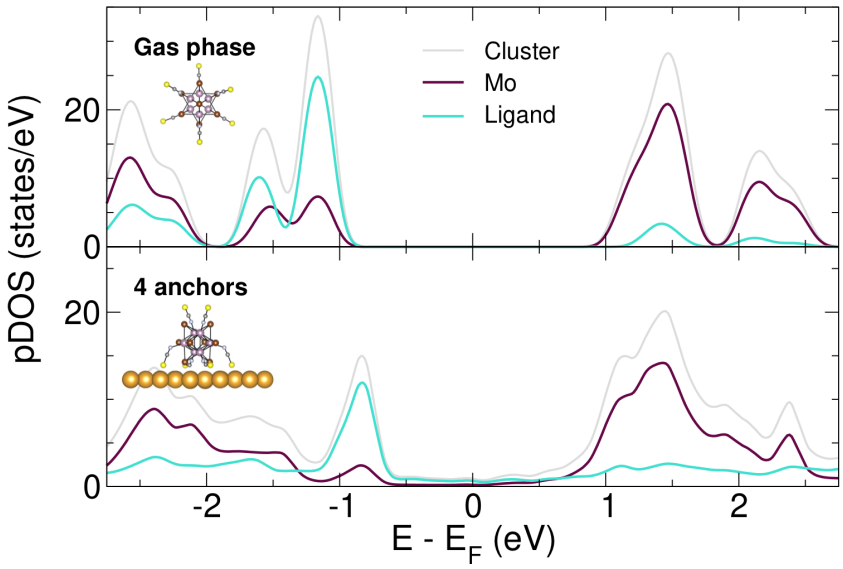


**Figure S10.** Density of states projected on $[Mo_6Br_8(NCS)_6]$ states (gray solid line) as well as on Mo (maroon solid line) and NCS-ligands (blue solid line) states in the gas phase molecular cluster (top) and the grafted surface (bottom).

# References


[1] K. Kirakci, S. Cordier and C. Perrin, *Z. Anorg. Allg. Chem.*, 2005, **631**, 411–416.

[2] *APEX3 program suite V2016.1-0, Bruker AXS Inc., Wisconsin, USA*.

[3] G. M. Sheldrick, *SAINT version 8.37A, Bruker AXS Inc., Wisconsin, USA, 2013*.

[4] G. M. Sheldrick, *SADABS version 2014/5, SADABS Bruker AXS Inc., Madison, Wisconsin, USA*.

[5] A. Altomare, M. C. Burla, M. Camalli, G. L. Cascarano, C. Giacovazzo, A. Guagliardi, A. G. G. Moliterni, G. Polidori and R. Spagna, *J. Appl. Cryst.*, 1999, **32**, 115–119.

[6] G. M. Sheldrick, *Acta Cryst.*, 2015, **C71**, 3–8.

[7] L. Farrugia, *J. Appl. Crystallogr.*, 2012, **45**, 849–854.

[8] M. Sicot, S. Andrieu, P. Turban, Y. Fagot-Revurat, H. Cercellier, A. Tagliaferri, C. De Nadai, N. B. Bookes, F. Bertran and F. Fortuna, *Phys. Rev. B*, 2003, **68**, 184406.

[9] N. Prokopuk and D. F. Shriver, *Chem. Mater.*, 1999, **11**, 1230–1236.

[10] N. G. Connelly and W. E. Geiger, *Chem. Rev.*, 1996, **96**, 877–910.

[11] J. M. Soler, E. Artacho, J. D. Gale, A. García, J. Junquera, P. Ordejón and D. Sánchez-Portal, *J. Phys.: Condens. Matter*, 2002, **14**, 2745–2779.

[12] E. Artacho, E. Anglada, O. Diéguez, J. D. Gale, A. García, J. Junquera, R. M. Martin, P. Ordejón, J. M. Pruneda, D. Sánchez-Portal and J. M. Soler, *J. Phys.: Condens. Matter*, 2008, **20**, 064208.

[13] Y. Zhang and W. Yang, *Phys. Rev. Lett.*, 1998, **80**, 890.

[14] N. Troullier and J. L. Martins, *Phys. Rev. B*, 1991, **43**, 1993–2006.

[15] E. Artacho, D. Sánchez-Portal, P. Ordejón, A. García and J. M. Soler, *phys. stat. sol. (b)*, 1999, **215**, 809–817.

[16] G. te Velde, F. M. Bickelhaupt, E. J. Baerends, C. Fonseca Guerra, S. J. A. van Gisbergen, J. G. Snijders and T. Ziegler, *J. Comput. Chem.*, 2001, **22**, 931–967.

[17] C. Fonseca Guerra, J. G. Snijders, G. te Velde and E. J. Baerends, *Theor. Chem. Acc.*, 1998, **99**, 391–403.

[18] E. van Lenthe, A. Ehlers and E. J. Baerends, *J. Chem. Phys.*, 1999, **110**, 8943–8952.

[19] E. van Lenthe and E. J. Baerends, *J. Comput. Chem.*, 2003, **24**, 1142–1156.

[20] K. Costuas, A. Garreau, A. Bulou, B. Fontaine, J. Cuny, R. Gautier, M. Mortier, Y. Molard, J.-L. Duvail, E. Faulques and S. Cordier, *Phys. Chem. Chem. Phys.*, 2015, **17**, 28574–28585.

[21] A. J. Bard and L. R. Faulkner, *Electrochemical Methods. Fundamentals and Applications*, Wiley, New York, 1980.

[22] R. Ramirez-Tagle and R. Arratia-Pérez, *Chem. Phys. Lett.*, 2008, **455**, 38–41.